PERGAMON

International Journal of Solids and Structures 36 (1999) 3051–3071

INTERNATIONAL JOURNAL OF SOLIDS and STRUCTURES

Steady-state limit analysis of elastoplastic trusses under cyclic loads

K. Uetani, Y. Araki*

Department of Architecture and Architectural Systems, Graduate School of Engineering, Kyoto University, Sakyo, Kyoto 606-8317, Japan

Received 7 October 1997; in revised form 7 April 1998

Abstract

For elastoplastic trusses under cyclic loads, a method is presented for finding the steady-state limit, which bounds convergence and divergence of plastic deformations. Using Taylor-series expansion, a new incremental theory is formulated for tracing the sequence of steady states generated under an idealized cyclic loading program with continuously increasing amplitude. The sequence is regarded as a continuous path. The steady-state limit is found as the first limit point of the continuous path. Geometrical and material nonlinearities are taken into account using the Total Lagrangian formulation and the bi-linear kinematic hardening rule. Validity of the proposed method is shown through numerical examples.

1. Introduction

Under cyclic bending with stepwisely increasing amplitude in the presence of a certain compressive axial force, it is known through experiments (Uetani and Nakamura, 1983) that a cantilever beam-column exhibits the following consecutive three classes of behavior as shown in Fig. 1: (1) convergent behavior to a symmetric steady-state, in which a pair of the deflected configurations at load reversals is symmetric with respect to the initial member axis; (2) convergent behavior to an asymmetric steady-state, where the deflected shapes involve a certain anti-symmetric mode; (3) divergent behavior, which is referred to as cyclic instability in this paper, where the deformation grows proportionally or exponentially with respect to the number of cycles. The concepts, called the symmetry limit and the steady-state limit, were introduced as the critical steady states that bound these three classes of behavior. The symmetry limit is the critical steady state at which transition from the symmetric steady state to the asymmetric steady state occurs. The steady-state limit is the critical steady state beyond which the beam-column will no longer exhibit any convergent

* Corresponding author. Fax: 00 81 757535757; E-mail: araki@archi.kyoto-u.ac.jp

0020–7683/99/$ - see front matter
PII: S0020–7683(98)00140–1

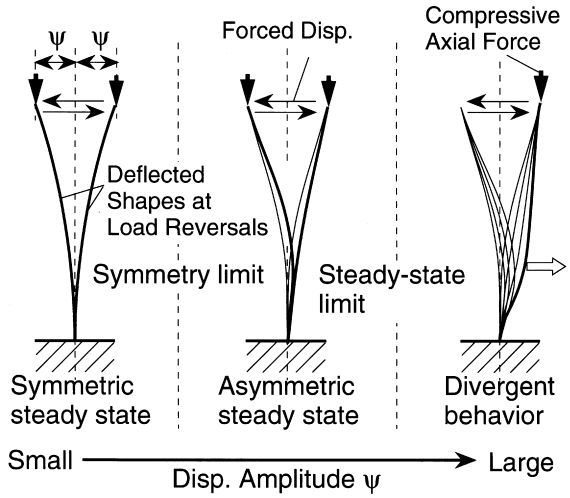

Fig. 1. The symmetry limit and the steady-state limit of a cantilever beam-column.

behavior. To predict the symmetry limit and the steady-state limit, the symmetry limit theory and the steady-state limit theory were developed, respectively (Uetani and Nakamura, 1983; Uetani, 1984; Uetani, 1989).

It might be thought that the symmetry limit and the steady-state limit can be found by applying the previously established theories. Nevertheless, none of them are directly applicable for the following reasons: (1) plastic buckling theory (Shanley, 1947; Hill, 1958; Bazant and Cedolin, 1991): the symmetry limit and the steady-state limit are phenomenologically and conceptually different from the critical point, such as a branching point or a limit point, of the equilibrium path. In other words, the cyclic instability may take place without passing these critical equilibrium points; (2) shakedown theory and its extensions: the symmetry limit and the steady-state limit are observed under the strong effect of geometrical nonlinearity. In the classical shakedown theory (Koiter, 1960; König, 1987), however, geometrical nonlinearity is completely neglected. Several papers (Maier, 1972; Nguyen et al., 1983; Siemaszko and König, 1985; Weichert, 1986; Gross-Weege, 1990; Pycko and König, 1991; Stumpf, 1993; Polizzotto and Borio, 1996) extended the classical shakedown theory by taking the geometrical nonlinearity into account. Nonetheless the extended shakedown theories, except the theory by Stumpf (1993) which essentially requires a numerical response analysis, are not valid when compressive stresses and/or large deformations have strong influence on the structural response; (3) numerical methods for response analysis: it is possible to bound convergence and divergence of plastic deformations by tracing all loading histories with response analysis (see e.g. Maier et al., 1993). But a number of parametric analyses are required for bounding the structural responses. Moreover, the parametric analyses will never lead to any theoretical condition similar to that for the Euler load.

On the other hand, in the symmetry limit theory and the steady-state limit theory, these two limits are found based on the following concepts. First, a steady state is considered as a point in a special space schematically illustrated in Fig. 2. Second, the sequence of these points, generated under an idealized cyclic loading program with continuously increasing amplitude, is regarded as

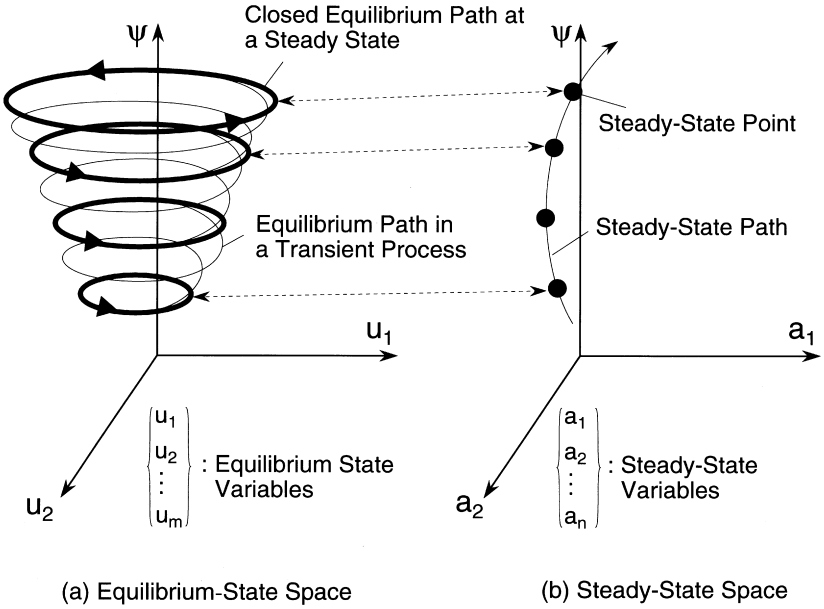

Fig. 2. The equilibrium-state space and the steady-state space.

a continuous path. This path is called the steady-state path. Third, the symmetry limit and the steady-state limit are found, respectively, as the first branching point and the first limit point of the steady-state path as shown in Fig. 3. Since only the sequence of the steady states is traced, there is no need for tracing the transient process between any pair of two adjacent steady states.

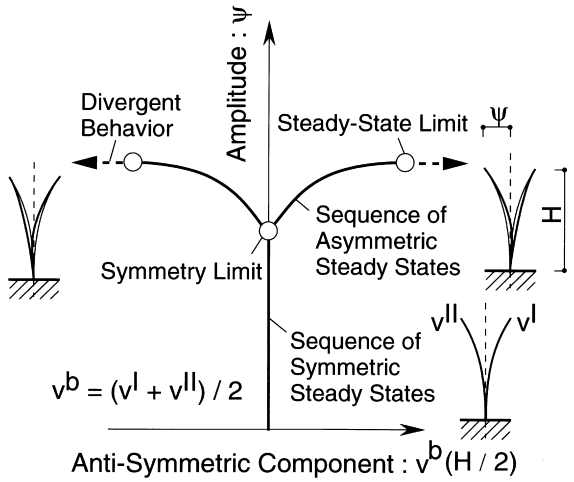

Fig. 3. The symmetry limit and the steady-state limit in a steady-state plane.

Furthermore, no parametric analysis is needed to detect the two limits because they are predicted as the critical points of the steady-state path.

For a few classes of structures, the symmetry limit theory and the steady-state limit theory have been applied. It was shown that severe cyclic instability is induced when the deflection amplitude is in excess of the symmetry limit or the steady-state limit (Uetani, 1984, 1991). In those studies, however, only simple structures, e.g. a cantilever beam-column or a unit frame, were treated for which analytical solutions can be derived. Hence, to investigate the limit states of more complex and practical structures, which generally do not have a symmetry limit if they do not have a symmetric shape, it is necessary to establish a method for predicting the steady-state limit using an appropriate finite element method.

The purpose of this paper is to present a new method for finding the steady-state limit of elastoplastic trusses, which are one of the simplest finite-dimensional structures, subjected to initial constant loads and subsequent cyclic loads. In the following sections, governing equations are described first. Then the fundamental concepts of the steady-state limit theory are shown. Next, using the Taylor-series expansion, a new incremental theory is formulated for tracing the steady-state path. Finally, validity of the proposed method is demonstrated through numerical examples. For simplicity, our consideration is restricted to the case in which dynamic and thermal effects can be neglected. In addition, the scope of this paper is limited to an elastic shakedown region because the problem becomes much more complicated when plastic shakedown occurs in the trusses. Throughout this paper, as referred in recent papers (see e.g. Maier et al., 1993), elastic shakedown or classic shakedown means a cyclic and fully elastic structural response after some history of plastic deformations. And plastic shakedown is so called alternating plasticity, in which plastic deformations are included in steady cycles.

2. Governing equations

2.1. Analytical model

Consider a space truss with M elements and N nodes. Compatibility conditions, equilibrium conditions and constitutive relations are given for an element shown in Fig. 4. By assembling the equilibrium equations for the element, we have those for the total system. Note that buckling of the element is ruled out though buckling of a global type is taken into account using a nonlinear strain–displacement relation.

We measure stresses and strains using the Total Lagrangian formulation (see e.g. Crisfield, 1991; Bathe, 1996). Assumptions of large displacements–small strains are employed. Green–Lagrangian strain ε is expressed as

$$\varepsilon = \frac{L^2 - L_0^2}{2L_0^2} \tag{1}$$

where L and L_0 are the current length and the initial length of the element, respectively. The relations between the current length L and the nodal displacement u_i is written as

$$L^2 = (x_4 - x_1)^2 + (x_5 - x_2)^2 + (x_6 - x_3)^2 \tag{2}$$

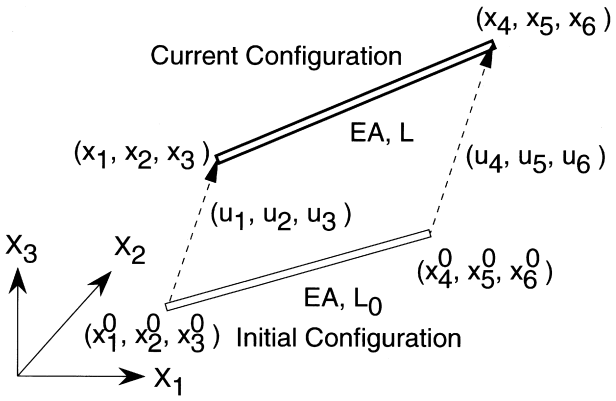

Fig. 4. A space truss element.

$$x_i = x_i^0 + u_i; \quad i = 1, \ldots, 6 \tag{3}$$

in which x_i and x_i^0 indicate the current position and the initial position of the nodes at the two ends, respectively, as illustrated in Fig. 4.

The principle of virtual work for the element is given by

$$f_i \delta u_i = \int_V \sigma \delta\varepsilon \, \mathrm{d}V = AL_0 \sigma \frac{\partial \varepsilon}{\partial u_i} \delta u_i \tag{4}$$

where f_i is the nodal force, δu_i is the virtual nodal displacement, V is the initial volume, σ is the second Piola–Kirchhoff stress, $\delta\varepsilon$ is the virtual strain, and A is the initial cross sectional area. Note that the summation convention is used only for the subscripts i, j and k throughout this paper. Since the virtual work eqn (4) should be satisfied for any δu_i, we obtain the equilibrium equation

$$f_i = AL_0 \sigma \frac{\partial \varepsilon}{\partial u_i}. \tag{5}$$

As a uni-axial constitutive relation for the truss element, we use a bi-linear kinematic hardening rule shown in Fig. 5. In terms of Young's modulus E, the tangent modulus after yielding E_t, the initial tensile yield stress σ_y, and the plastic strain ε_p, the constitutive law is expressed as follows:

$$\sigma = E(\varepsilon - \varepsilon_p) \quad \text{in the elastic and unloading ranges,} \tag{6}$$

$$\sigma = E_t \varepsilon + \bar{\sigma}_y \quad \text{for the plastic loading in tension,} \tag{7}$$

$$\sigma = E_t \varepsilon - \bar{\sigma}_y \quad \text{for the plastic loading in compression} \tag{8}$$

where $\bar{\sigma}_y = (1 - E_t/E)\sigma_y$.

2.2. Cyclic responses

For later formulation of the steady-state limit theory, we must examine all the possible types of the cyclic responses in the stress–strain plane. The possible cyclic responses are classified into four

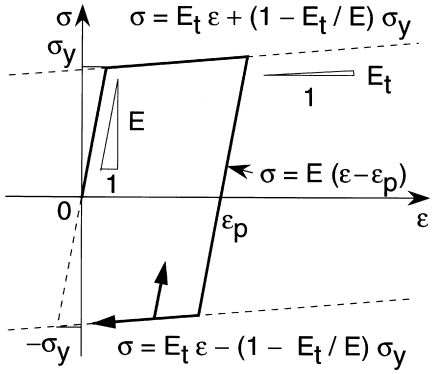

Fig. 5. A bi-linear kinematic hardening rule.

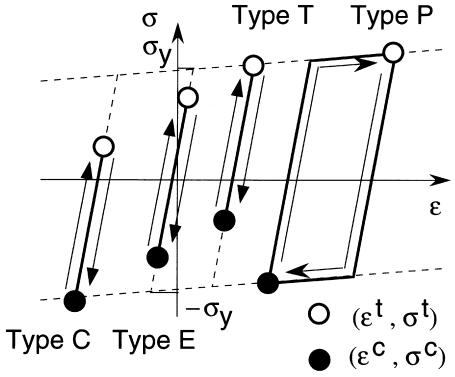

Fig. 6. Possible types of cyclic responses.

different types E, C, T and P as shown in Fig. 6, where the superscripts t and c indicate the state variables, such as stresses, strains, and displacements, at strain reversals in tension and compression, respectively. In terms of $(\varepsilon^t, \sigma^t)$ and $(\varepsilon^c, \sigma^c)$, the cyclic responses can be uniquely described as:

$$\sigma^t = E(\varepsilon^t - \varepsilon_p^t), \tag{9}$$

$$\sigma^c = E(\varepsilon^c - \varepsilon_p^c), \tag{10}$$

for type E, which represents a purely elastic response or an elastic shakedown state.

$$\sigma^t = E_t\varepsilon^t + \bar{\sigma}_y, \tag{11}$$

$$\sigma^c = (E_t - E)\varepsilon^t + E\varepsilon^c + \bar{\sigma}_y \tag{12}$$

for type T, which is the elastic shakedown state whose maximum stress reaches the tensile yield stress.

$$\sigma^t = E\varepsilon^t + (E_t - E)\varepsilon^c + \bar{\sigma}_y, \tag{13}$$

$$\sigma^c = E_t\varepsilon^c - \bar{\sigma}_y \tag{14}$$

for type C, which represents the elastic shakedown state that starts from and reaches the compressive strain hardening line. And

$$\sigma^t = E_t\varepsilon^t + \bar{\sigma}_y, \tag{15}$$

$$\sigma^c = E_t\varepsilon^c - \bar{\sigma}_y \tag{16}$$

for type P, which indicates the plastic shakedown state. Though all the possible types are shown here, the type P is not considered in this paper because the discussion is limited to the elastic shakedown region as mentioned in Introduction.

Note that the plastic strain ε_p is eliminated in eqns (12) and (13). For type T, σ^t is expressed in two ways using eqns (6) and (7), while σ^c is written using only eqn (6). The plastic strains at the strain reversals are eliminated using these three expressions and the relation

$$\varepsilon_p^t = \varepsilon_p^c. \tag{17}$$

For type C, the plastic strains can be eliminated similarly.

3. Fundamental concepts

3.1. Loading conditions

The truss is subjected to initial constant loads $\lambda_0\bar{\mathbf{P}}_0$ and subsequent cyclic loads $\lambda_c\bar{\mathbf{P}}_c$. Here, λ and $\bar{\mathbf{P}}$ denote the load factor and the constant vector, respectively. The subscripts 0 and c indicate that the variables refer to the constant loads and to the cyclic loads, respectively. External forces and/or forced displacements are applied as the external loads. In other words, nodal forces and/or nodal displacements are included in $\bar{\mathbf{P}}$ according to the boundary conditions. The load factor λ_c is varied between the maximum value $\lambda_c^{\mathrm{I}} = \psi$ and the minimum value $\lambda_c^{\mathrm{II}} = -\psi$ in a cycle, where ψ denotes the amplitude of λ_c. The equilibrium states at which $\lambda_c = \lambda_c^{\mathrm{I}}$ and $\lambda_c = \lambda_c^{\mathrm{II}}$ are called Γ^{I} state and Γ^{II} state, respectively. The superscripts I and II indicate that the state variables refer to those for the Γ^{I} and Γ^{II} states, respectively.

Let us define the cyclic loading program. As a preliminary program, consider a cyclic loading program shown in Fig. 7(a). In the program, the loading cycle is repeated as many times as necessary for the truss to converge to a steady state. After convergence, a small increment $\Delta\psi$ is added. A sequence of the steady states is generated under the cyclic loading program as shown in Fig. 2. By taking the limit $\Delta\psi \to 0$ as illustrated in Fig. 7(b), the sequence of the points can be considered as a continuous path as depicted in Fig. 2(b). The continuous path is called steady-state path. The steady-state path is defined by a monotonically increasing parameter τ, called steady-state path parameter.

3.2. Hypotheses

To formulate directly the sequence of the steady states in terms of the state variables for Γ^{I} and Γ^{II}, the following hypotheses are introduced:

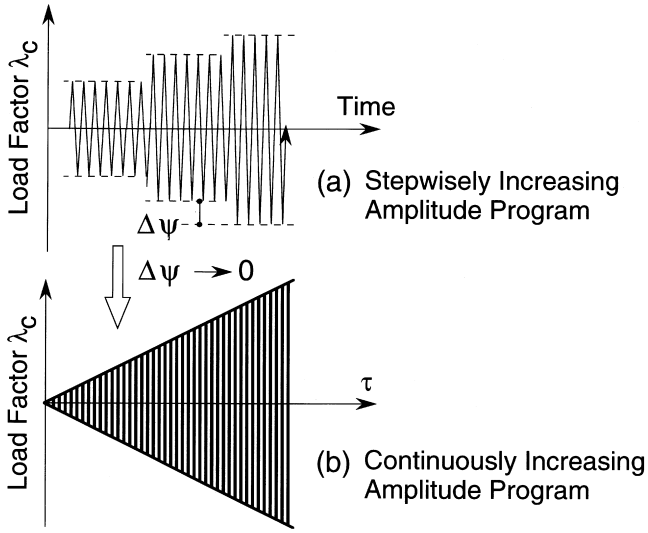

Fig. 7. Idealized cyclic loading programs.

(H2*) All the state variables for Γ^{I} and Γ^{II} are continuous and piecewise differentiable functions of τ.
(H3*) For all elements, strain reversals occur only at Γ^{I} or Γ^{II}.

The hypotheses (H2*) and (H3*) are the alternative statements of the hypotheses (H2) and (H3), respectively, introduced by Uetani and Nakamura (1983). Note that the hypothesis (H3*) is applied not for the transient response between the two consecutive steady states but for the steady-state response after convergence.

3.3. Outline

Based on these hypotheses, the procedures for finding the steady-state limit are outlined as follows:

(1) A steady-state is uniquely described by a set of the state variables for Γ^{I} and Γ^{II}.
(2) The steady-state path is traced based on an incremental theory for variation of steady states, where the state variables for Γ^{I} and Γ^{II} are differentiated with respect to τ.
(3) The steady-state limit is found as the first limit point of the steady-state path.

4. Formulation

4.1. Incremental theory for variation of steady state

When all the state variables are known for the current steady states at $\tau = \tau_h$, the problem is then to determine those for a neighboring steady state at $\tau = \tau_{h+1}$. Let $\Delta\tau = \tau_{h+1} - \tau_h$ be an

increment of the steady-state path parameter τ. Then, on the basis of the hypothesis (H2*), the state variables for Γ^{I} at $\tau = \tau_{h+1}$ are expressed using the Taylor-series expansion as:

$$\mathbf{U}^{\mathrm{I}}(\tau_{h+1}) = \mathbf{U}^{\mathrm{I}}(\tau_h) + \dot{\mathbf{U}}^{\mathrm{I}}(\tau_h)\Delta\tau + \tfrac{1}{2}\ddot{\mathbf{U}}^{\mathrm{I}}(\tau_h)\Delta\tau^2 + \cdots, \tag{18}$$

$$\mathbf{F}^{\mathrm{I}}(\tau_{h+1}) = \mathbf{F}^{\mathrm{I}}(\tau_h) + \dot{\mathbf{F}}^{\mathrm{I}}(\tau_h)\Delta\tau + \tfrac{1}{2}\ddot{\mathbf{F}}^{\mathrm{I}}(\tau_h)\Delta\tau^2 + \cdots, \tag{19}$$

$$\mathbf{E}^{\mathrm{I}}(\tau_{h+1}) = \mathbf{E}^{\mathrm{I}}(\tau_h) + \dot{\mathbf{E}}^{\mathrm{I}}(\tau_h)\Delta\tau + \tfrac{1}{2}\ddot{\mathbf{E}}^{\mathrm{I}}(\tau_h)\Delta\tau^2 + \cdots, \tag{20}$$

$$\mathbf{E}_p^{\mathrm{I}}(\tau_{h+1}) = \mathbf{E}_p^{\mathrm{I}}(\tau_h) + \dot{\mathbf{E}}_p^{\mathrm{I}}(\tau_h)\Delta\tau + \tfrac{1}{2}\ddot{\mathbf{E}}_p^{\mathrm{I}}(\tau_h)\Delta\tau^2 + \cdots, \tag{21}$$

$$\mathbf{S}^{\mathrm{I}}(\tau_{h+1}) = \mathbf{S}^{\mathrm{I}}(\tau_h) + \dot{\mathbf{S}}^{\mathrm{I}}(\tau_h)\Delta\tau + \tfrac{1}{2}\ddot{\mathbf{S}}^{\mathrm{I}}(\tau_h)\Delta\tau^2 + \cdots \tag{22}$$

where $\mathbf{F}$ and $\mathbf{U}$ are the nodal force vector and the nodal displacement vector, respectively, with $3N$ components, and $\mathbf{E}$, $\mathbf{E}_p$ and $\mathbf{S}$ denote the strain vector, the plastic strain vector, and the stress vector, respectively, with M components. The super dot indicates the differentiation with respect to τ. The variables for Γ^{II} are expressed by replacing the superscript I with II.

For simple presentation of the incremental theory, only the formulation is shown here in which the terms higher than or equal to the second order are neglected. However, since it is desirable to use a more accurate solution method for this highly nonlinear system, the formulation including the higher-order derivatives is presented in Appendix A.

4.2. Rate forms of governing equations

By differentiating all the governing equations for Γ^{I} and Γ^{II} with respect to the steady-state parameter τ, we derive the rate forms of the governing equations. The rate forms of the governing equations are simply called the rate equations in this paper. Differentiation of the compatibility conditions (1)–(3) yields

$$\dot{\varepsilon}^{\mathrm{I}} = \frac{\partial \varepsilon^{\mathrm{I}}}{\partial u_i^{\mathrm{I}}}\dot{u}_i^{\mathrm{I}}, \tag{23}$$

$$\dot{\varepsilon}^{\mathrm{II}} = \frac{\partial \varepsilon^{\mathrm{II}}}{\partial u_i^{\mathrm{II}}}\dot{u}_i^{\mathrm{II}}. \tag{24}$$

Recall that summation convention is used only for the subscripts i, j and k which are varied from 1 to 6. Rate forms of the equilibrium conditions are given by

$$\dot{f}_i^{\mathrm{I}} = AL_0\left(\dot{\sigma}^{\mathrm{I}}\frac{\partial \varepsilon^{\mathrm{I}}}{\partial u_i^{\mathrm{I}}} + \sigma^{\mathrm{I}}\frac{\partial^2 \varepsilon^{\mathrm{I}}}{\partial u_i^{\mathrm{I}}\,\partial u_j^{\mathrm{I}}}\dot{u}_j^{\mathrm{I}}\right), \tag{25}$$

$$\dot{f}_i^{\mathrm{II}} = AL_0\left(\dot{\sigma}^{\mathrm{II}}\frac{\partial \varepsilon^{\mathrm{II}}}{\partial u_i^{\mathrm{II}}} + \sigma^{\mathrm{II}}\frac{\partial^2 \varepsilon^{\mathrm{II}}}{\partial u_i^{\mathrm{II}}\,\partial u_j^{\mathrm{II}}}\dot{u}_j^{\mathrm{II}}\right). \tag{26}$$

Differentiating the stress–strain relations (9)–(12), the stress rate–strain rate relations can be expressed for the strain–reversal points in the form of

Table 1
Stress rate–strain rate relations for strain–reversal points

Type	Strain rate	C^{tt}	C^{tc}	C^{ct}	C^{cc}
E		E	0	0	E
T	$\dot{\varepsilon}^t \geqslant 0$	E_t	0	$E_t - E$	E
T	$\dot{\varepsilon}^t < 0$	E	0	0	E
C	$\dot{\varepsilon}^c \leqslant 0$	E	$E_t - E$	0	E_t
C	$\dot{\varepsilon}^c > 0$	E	0	0	E

$$\dot{\sigma}^t = C^{tt}\dot{\varepsilon}^t + C^{tc}\dot{\varepsilon}^c, \tag{27}$$

$$\dot{\sigma}^c = C^{ct}\dot{\varepsilon}^t + C^{cc}\dot{\varepsilon}^c, \tag{28}$$

where C^{cc}, C^{ct}, C^{tc} and C^{tt} are the coefficients that should be chosen according to the current type of the cyclic response. And the signs of the strain rates are shown in Table 1 and Fig. 8. It may be worth noting that the stress rate–strain rate relations are derived by differentiating eqns (9)–(14) in the proposed method. In contrast, they are obtained by differentiating eqns (6)–(8) in the conventional methods for response analysis.

To derive the rate equations for Γ^{I} and Γ^{II}, eqns (27) and (28) for the strain–reversal points are transformed into those for the load–reversal points by replacing their superscripts on the basis of the hypothesis (H3*). The superscripts c and t are replaced by I and II, respectively, or they are replaced with II and I, respectively. After replacing the superscripts, we have

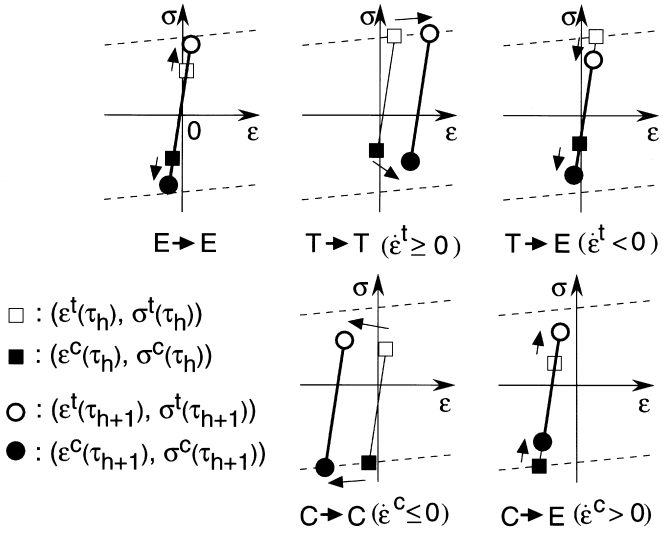

Fig. 8. Possible variation of cyclic responses.

$$\dot{\sigma} = C^{\mathrm{II}}\dot{\varepsilon}^{\mathrm{I}} + C^{\mathrm{I\,II}}\dot{\varepsilon}^{\mathrm{II}}, \tag{29}$$

$$\dot{\sigma}^{\mathrm{II}} = C^{\mathrm{II\,I}}\dot{\varepsilon}^{\mathrm{I}} + C^{\mathrm{II\,II}}\dot{\varepsilon}^{\mathrm{II}}. \tag{30}$$

Substituting eqns (23), (24), (29) and (30) into eqns (25) and (26), we have the rate equations for each element

$$\dot{f}_i^{\mathrm{I}} = k_{ij}^{\mathrm{II}}\dot{u}_j^{\mathrm{I}} + k_{ij}^{\mathrm{I\,II}}\dot{u}_j^{\mathrm{II}}, \tag{31}$$

$$\dot{f}_i^{\mathrm{II}} = k_{ij}^{\mathrm{II\,I}}\dot{u}_j^{\mathrm{I}} + k_{ij}^{\mathrm{II\,II}}\dot{u}_j^{\mathrm{II}}, \tag{32}$$

where

$$k_{ij}^{\mathrm{II}} = AL_0\left(C^{\mathrm{II}}\frac{\partial\varepsilon^{\mathrm{I}}}{\partial u_i^{\mathrm{I}}}\frac{\partial\varepsilon^{\mathrm{I}}}{\partial u_j^{\mathrm{I}}} + \sigma^{\mathrm{I}}\frac{\partial^2\varepsilon^{\mathrm{I}}}{\partial u_i^{\mathrm{I}}\,\partial u_j^{\mathrm{I}}}\right), \tag{33}$$

$$k_{ij}^{\mathrm{I\,II}} = AL_0C^{\mathrm{I\,II}}\frac{\partial\varepsilon^{\mathrm{I}}}{\partial u_i^{\mathrm{I}}}\frac{\partial\varepsilon^{\mathrm{II}}}{\partial u_j^{\mathrm{II}}}, \tag{34}$$

$$k_{ij}^{\mathrm{II\,I}} = AL_0C^{\mathrm{II\,I}}\frac{\partial\varepsilon^{\mathrm{II}}}{\partial u_i^{\mathrm{II}}}\frac{\partial\varepsilon^{\mathrm{I}}}{\partial u_j^{\mathrm{I}}}, \tag{35}$$

$$k_{ij}^{\mathrm{II\,II}} = AL_0\left(C^{\mathrm{II\,II}}\frac{\partial\varepsilon^{\mathrm{II}}}{\partial u_i^{\mathrm{II}}}\frac{\partial\varepsilon^{\mathrm{II}}}{\partial u_j^{\mathrm{II}}} + \sigma^{\mathrm{II}}\frac{\partial^2\varepsilon^{\mathrm{II}}}{\partial u_i^{\mathrm{II}}\,\partial u_j^{\mathrm{II}}}\right). \tag{36}$$

By assembling eqns (31) and (32) throughout the whole structure, the following rate equations are derived for the total system:

$$\dot{\mathbf{F}}^{\mathrm{I}} = \mathbf{K}^{\mathrm{II}}\dot{\mathbf{U}}^{\mathrm{I}} + \mathbf{K}^{\mathrm{I\,II}}\dot{\mathbf{U}}^{\mathrm{II}}, \tag{37}$$

$$\dot{\mathbf{F}}^{\mathrm{II}} = \mathbf{K}^{\mathrm{II\,I}}\dot{\mathbf{U}}^{\mathrm{I}} + \mathbf{K}^{\mathrm{II\,II}}\dot{\mathbf{U}}^{\mathrm{II}} \tag{38}$$

where $\mathbf{K}^{\mathrm{II}}$, $\mathbf{K}^{\mathrm{I\,II}}$, $\mathbf{K}^{\mathrm{II\,I}}$ and $\mathbf{K}^{\mathrm{II\,II}}$ are the coefficient matrices of the nodal displacement rates. By specifying the value of $\dot{\psi}$ and by using the boundary conditions, we have a system of $2\times 3N$ simultaneous linear equations.

4.3. Consistent set of stress rate–strain rate relations

When an element exhibits the type T or C in the current steady state, the coefficients of the strain rates should be chosen according to the signs of the strain rates as shown in Table 1 and Fig. 8. Therefore, for all the elements exhibiting the type T or C, we should choose a set of the coefficients that are consistent with the signs of the resulting strain rates. Note that the term consistent used here has no relation with the one used in the integration algorithms for the numerical response analysis of elastoplastic solids or structures (see e.g. Crisfield, 1997).

To find the consistent set of the coefficients, we employ a trial and error approach, which is also used in the conventional response analysis (Yokoo et al., 1976). In the trial and error approach, first, the signs of the strain rates $\dot{\mathbf{E}}^{\mathrm{I}}$ and $\dot{\mathbf{E}}^{\mathrm{II}}$ are assumed to be identical to those in the last step. Then, the coefficients C^{cc}, C^{ct}, C^{tc} and C^{tt} are determined according to the assumptions, and the

rate equations are constructed. After the rate equations are solved and $\dot{\mathbf{E}}^{\mathrm{I}}$ and $\dot{\mathbf{E}}^{\mathrm{II}}$ are calculated, the consistency is checked between the assumed and the resulting signs of the strain rates for all the elements exhibiting the type T or C. If the signs are not consistent, the assumed signs are reversed. This procedure is continued until all the resulting signs of the strain rates are consistent with the assumed ones.

4.4. Termination conditions for incremental steps

When the type of the stress–strain cyclic response changes, a different type of stress rate–strain rate relation should be used in eqns (29) and (30). The step length $\Delta\tau$ is, therefore, determined considering the conditions for the transition of the type of the stress–strain cyclic response. Let σ_{yt} and σ_{yc} denote the subsequent yield stresses in tension and compression, respectively. Then, for every element, $\Delta\tau$ is calculated using the following conditions:

$$\sigma^t(\tau_{h+1}) = \sigma_{yt}, \tag{39}$$

$$\sigma^c(\tau_{h+1}) = \sigma_{yc}, \tag{40}$$

$$\sigma^t(\tau_{h+1}) - \sigma^c(\tau_{h+1}) = \sigma_{yt} - \sigma_{yc} = 2\sigma_y \tag{41}$$

where $\sigma^t(\tau_{h+1}) = \sigma^t(\tau_h) + \dot{\sigma}^t(\tau_h)\Delta\tau$ and $\sigma^c(\tau_{h+1}) = \sigma^c(\tau_h) + \dot{\sigma}^c(\tau_h)\Delta\tau$ in the linear approximation. Here, the eqns (39)–(41) describe the conditions for the transition of the cyclic response for E → T, E → C, and E, C or T → P, respectively. Examples of the transition are given in Fig. 9. Note that the subsequent yield stresses are expressed in terms of the plastic strain at the current steady state as

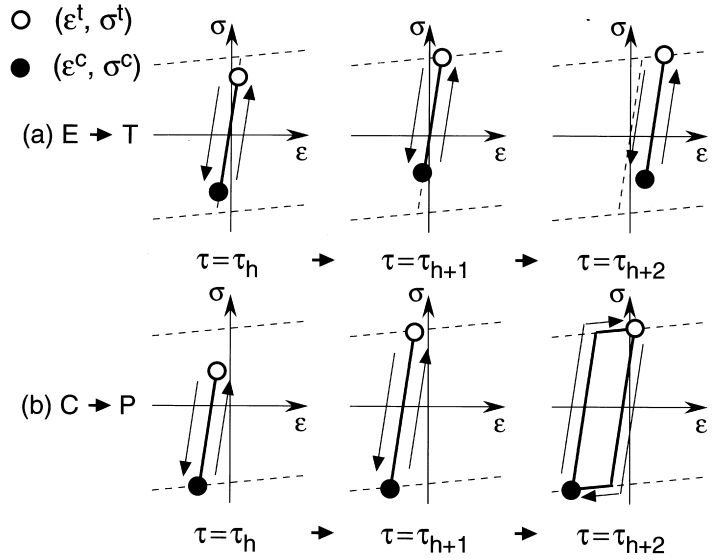

Fig. 9. Examples of transition of cyclic responses: (a) E → T and (b) C → P.

$$\sigma_{yt} = \frac{EE_t}{E-E_t}\varepsilon_p(\tau_h) + \sigma_y, \tag{42}$$

$$\sigma_{yc} = \frac{EE_t}{E-E_t}\varepsilon_p(\tau_h) - \sigma_y. \tag{43}$$

Besides the conditions above, the step length $\Delta\tau$ should be kept small enough to prevent excessive accumulation of truncation errors. Hence the step length $\Delta\tau$ is selected as the smallest value among the values calculated from the conditions (39)–(41) and the specified maximum allowable value $\Delta\bar{\tau}_{\max}$. When $\Delta\tau$ is determined by (39) or (40), the stress rate–strain rate relations are changed in the next step. If (41) is used to determine $\Delta\tau$, the incremental analysis is terminated.

4.5. Steady-state limit condition

Now, all the first-order derivatives and the step length $\Delta\tau$ have been obtained. Substituting $\Delta\tau$ and the first-order derivatives into eqns (18)–(22), we have all the state variables at $\tau = \tau_{h+1}$. Repeating these procedures, the steady-state path is traced incrementally.

As mentioned before, the steady-state limit is found as the first limit point of the steady-state path as shown in Fig. 3. The steady-state limit condition is given as

$$\dot{\psi} \leqslant 0. \tag{44}$$

Note that, to find the limit point and to trace the steady-state path after the limit point, a procedure should be employed similar to the displacement control schemes (Yokoo et al., 1976; Crisfield, 1991).

5. Numerical examples

The proposed method has been developed on the basis of the two hypotheses. In addition, the steady-state limit is predicted regardless of the transient process between two consecutive steady states. Hence validity of the two hypotheses and the steady-state limit should be examined. For this purpose, steady-state limit analysis and conventional response analysis, in which the entire history is traced, are carried out for a two-bar arch truss and a ten-bar cantilever truss.

5.1. Steady-state limit analysis

Initial shapes, boundary conditions and loading conditions of both plane trusses are illustrated in Fig. 10. The initial constant forces and the subsequent cyclic forced displacements are denoted by $\lambda_0\bar{F}_0$ and $\lambda_c\bar{U}_c$, respectively. Here, $\bar{F}_0 = 9.807 \times 10^3$ N and $\bar{U}_c = 1$ cm. The cross-sectional areas of the two-bar truss are $A_{(1)} = 1$ cm^2 and $A_{(2)} = 2$ cm^2, and those of the ten-bar truss are as follows: $A_{(1)} = A_{(4)} = A_{(5)} = 11$ cm^2, $A_{(2)} = A_{(3)} = 1.1$ cm^2, $A_{(6)} = A_{(9)} = A_{(10)} = 10$ cm^2, and $A_{(7)} = A_{(8)} = 1$ cm^2. Both trusses obey a bi-linear kinematic hardening rule with $E = 1.961 \times 10^2$ GPa, $E_t = 0.01E$, and $\sigma_y = 2.942 \times 10^2$ MPa. Throughout the steady-state limit analysis, higher-order terms up to the second order are incorporated (see Appendix A), and the maximum allowable step lengths are set to $\Delta\bar{\tau}_{\max} = 0.05$ and $\Delta\bar{\tau}_{\max} = 0.2$ for the two-bar truss and the ten-bar truss, respectively.

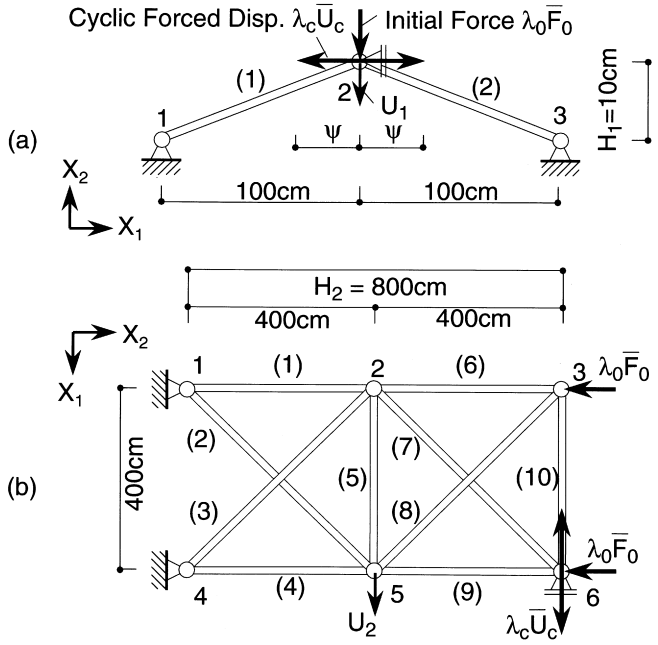

Fig. 10. The geometry of (a) a two-bar truss and (b) a ten-bar truss.

Let $\lambda_y\bar{F}_0$ and $\lambda_b\bar{F}_0$ denote the initial yield load and the initial buckling load, respectively, for the trusses subjected to only $\lambda_0\bar{F}_0$. As the results of the conventional response analysis, we have $\lambda_y = \lambda_b = 0.7477$ for the two-bar truss, and $\lambda_y = 30.96$ and $\lambda_b = 40.38$ for the ten-bar truss. Note that the term buckling means that the lowest eigenvalue of the tangent stiffness matrix for the Hill's linear comparison solid (Hill, 1958; Bazant and Cedolin, 1991) becomes non-positive in tracing the equilibrium path. In Hill's linear comparison solid, any yielding element is assumed to behave with their tangent stiffness for plastic loading even if its strain changes in an unloading direction.

Figures 11 and 12 illustrate the results of the steady-state limit analysis performed under different initial constant loads. The normalized load factor λ_0/λ_b is parametrically changed between 0 and 1 with the increments of 0.005 and 0.01 for the two-bar truss and the ten-bar truss, respectively. The solid line represents the steady-state limit ψ_{ssl} and the dashed line shows the boundary between the elastic shakedown region and the plastic shakedown region.

5.2. Response analysis

It is very difficult to realize the idealized cyclic loading program employed in the steady-state limit analysis. For the verification, therefore, we use the following two realistic loading programs shown in Fig. 13: (1) STIDAC program. The amplitude ψ of the forced displacement is increased every half cycle with an increment $\Delta\bar{\psi}$ from zero to a specified value $\bar{\psi}_{\max}$, then ψ is kept constant in the following cycles; (2) STIDAD program. Throughout all cycles, ψ is kept a constant value $\bar{\psi}$. The values of $\bar{\psi}_{\max}$ are set so as to be just below and above that of ψ_{ssl}. The values of $\bar{\psi}$ are set

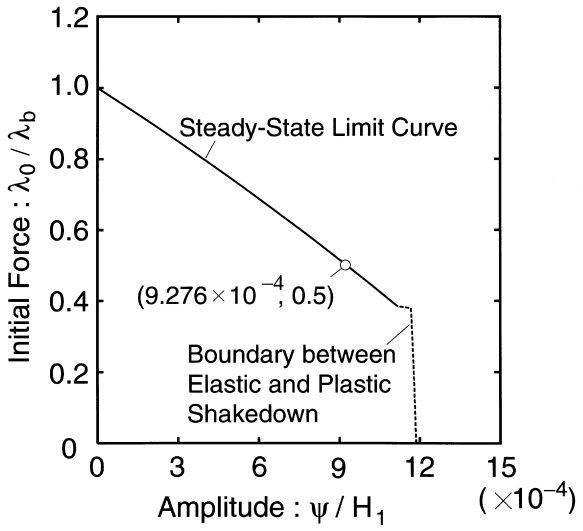

Fig. 11. The elastic shakedown boundaries for the two-bar truss.

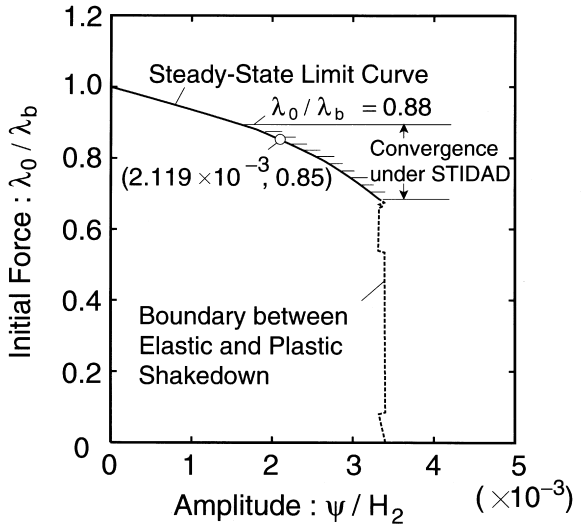

Fig. 12. The elastic shakedown boundaries for the ten-bar truss.

similarly. Consequently, the response analysis is performed four times for all the values of ψ_{ssl}. Formulation for the response analysis and criteria for convergence and divergence are shown in Appendix B.

For both of the trusses, the steady-state limit predicted by the proposed method is in good agreement with the results of the response analysis performed under the STIDAC program with $\bar{\psi}_{\max} = (1 \pm 0.001)\psi_{ssl}$ and $\Delta\bar{\psi} = 0.001\psi_{ssl}$. Namely, the convergence is observed if $\bar{\psi}_{\max} < \psi_{ssl}$ and,

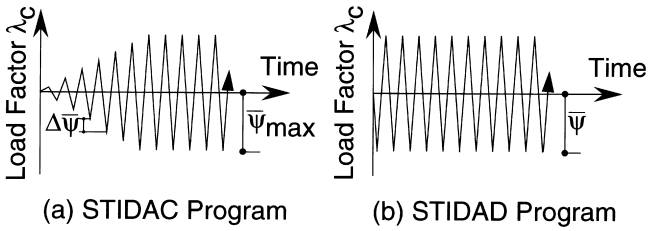

Fig. 13. The cyclic loading programs: (a) STIDAC and (B) STIDAD.

otherwise, divergence is obtained. Obviously, the program STIDAC become closer to the idealized program employed in the steady-state limit analysis as $\Delta\psi$ is made smaller. It may be therefore concluded that the steady state limit obtained by the proposed method is directly verified.

On the other hand, under the STIDAD program with $\bar{\psi} = (1 \pm 0.001)\psi_{ssl}$, the ten-bar truss converges to elastic shakedown state in the hatched range in Fig. 12 regardless of $\bar{\psi} > \psi_{ssl}$. However, such inconsistent results are obtained only when $\bar{\psi} > \psi_{ssl}$. From these results, it is observed that the value of the steady-state limit ψ_{ssl}, defined for the idealized cyclic loading program, is smaller than the limiting value of $\bar{\psi}$ that bounds convergence and divergence under the STIDAD program.

In Fig. 14, the relation between the vertical displacement U_1^{I} and the number of the cycles is plotted for the two-bar truss subjected to the STIDAD program with the four constant amplitudes $\bar{\psi}/\psi_{ssl} = 0.80$, 0.99, 1.01 and 1.05 under the initial loads $\lambda_0/\lambda_b = 0.5$. It can be observed from Fig. 14 that cyclic instability occurs if the amplitude ψ is above the predicted value of ψ_{ssl}, whereas U_1^{I} converges otherwise.

Figure 15 illustrates the comparison of the results for the ten-bar truss obtained by the steady-state limit analysis and the response analyses performed under various cyclic loading programs under the initial constant load $\lambda_0/\lambda_b = 0.85$. This figure shows the path-dependence of the limiting values that bound convergence and divergence on loading history. In the figure, U_2 is the dis-

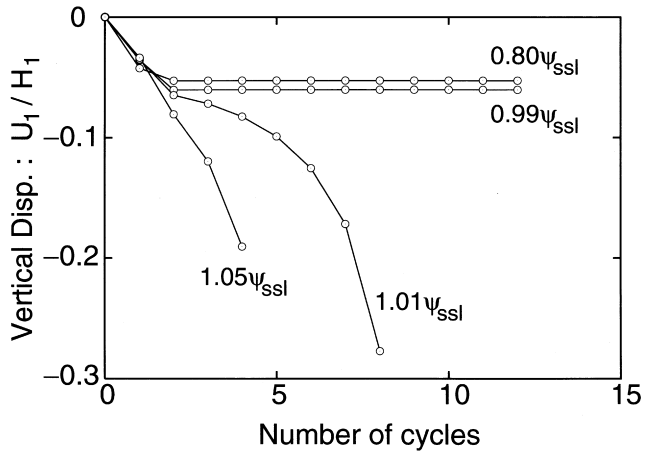

Fig. 14. Convergence and divergence of U_1^{I} for the two-bar truss ($\lambda/\lambda_b = 0.5$).

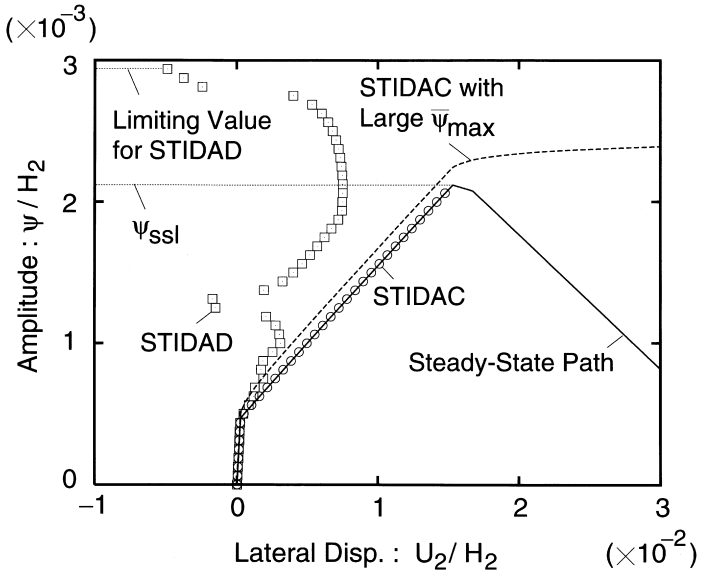

Fig. 15. Path dependence of U_1^{I} on loading history for the ten-bar trusses ($\lambda/\lambda_b = 0.85$).

placement of node 5 for X_1 direction. The solid line indicates the steady-state path. The dashed line shows the variation of U_2^{I} with respect to ψ under the STIDAC program with $\Delta\bar{\psi} = 0.001\psi_{ssl}$ and a sufficiently large value of $\bar{\psi}_{\max}$. The circular symbols plot U_2^{I} in the steady states under the STIDAC programs with $\Delta\bar{\psi} = 0.001\psi_{ssl}$ and various values of $\bar{\psi}_{\max}$. The square symbols indicate U_2^{I} after convergence under the STIDAD programs with the values of $\bar{\psi}$ corresponding to the values of $\bar{\psi}_{\max}$. Good agreement between the steady-state path and the circular points demonstrates the validity of the hypotheses (H2*) and (H3*).

6. Conclusions

A new method has been presented for predicting the steady-state limit of elastoplastic trusses subjected to quasi-static cyclic loads in the presence of constant loads. By applying the proposed method, we can find the steady-state limit of arbitrary shaped frames with truss elements. In the proposed method, there is no need for tracing the transient process between consecutive two steady states, and no parametric analysis is needed for finding the steady-state limit. The proposed method is therefore much more efficient than the conventional methods for numerical response analysis.

Through the numerical examples, the following conclusions have been obtained:

(1) Good agreement is observed between the results of the steady-state limit analysis and those of the conventional response analysis when the loading conditions for these analyses are close enough.
(2) The limiting values below which elastic shakedown occurs depend on the loading history.

Obviously, Melan-type or path-independent shakedown criterion cannot be extended to such cases.

(3) The steady-state limit, defined under an idealized cyclic loading program with continuously increasing amplitude, is smaller than the limiting values obtained by the response analysis performed under the two typical and realistic cyclic loading programs.

Extension of the proposed method to the plastic shakedown region is our next subject. Further extension to the three-dimensional continua remains as a subject of our future research.

Appendix A: Formulation with higher-order derivatives

A formulation with higher-order derivatives is presented for the steady-state limit analysis. By using the higher-order derivatives, terminal points of incremental steps can be found with the desired accuracy. We derive here only the second-order derivatives for brevity. But the higher-order derivatives can be obtained similarly.

Differentiation of the rate equations (23)–(30) with respect to the steady-state path parameter τ yields the second-order perturbation equations as follows:

$$\ddot{\varepsilon}^{\mathrm{I}} = \frac{\partial \varepsilon^{\mathrm{I}}}{\partial u_i^{\mathrm{I}}} \ddot{u}_i^{\mathrm{I}} + \frac{\partial^2 \varepsilon^{\mathrm{I}}}{\partial u_i^{\mathrm{I}} \partial u_j^{\mathrm{I}}} \dot{u}_i^{\mathrm{I}} \dot{u}_j^{\mathrm{I}} \tag{A1}$$

for the compatibility conditions,

$$\ddot{f}_i^{\mathrm{I}} = AL_0 \left\{ \ddot{\sigma}^{\mathrm{I}} \frac{\partial \varepsilon^{\mathrm{I}}}{\partial u_i^{\mathrm{I}}} + \sigma^{\mathrm{I}} \frac{\partial^2 \varepsilon^{\mathrm{I}}}{\partial u_i^{\mathrm{I}} \partial u_j^{\mathrm{I}}} \ddot{u}_j^{\mathrm{I}} + 2\dot{\sigma}^{\mathrm{I}} \frac{\partial^2 \varepsilon^{\mathrm{I}}}{\partial u_i^{\mathrm{I}} \partial u_j^{\mathrm{I}}} \dot{u}_j^{\mathrm{I}} \right\} \tag{A2}$$

for the equilibrium conditions, and

$$\ddot{\sigma}^{\mathrm{I}} = C^{\mathrm{II}} \ddot{\varepsilon}^{\mathrm{I}} + C^{\mathrm{I\,II}} \ddot{\varepsilon}^{\mathrm{II}} \tag{A3}$$

for the stress–strain relations. Note that $\dot{C}^{\mathrm{II}} = \dot{C}^{\mathrm{I\,II}} = 0$ because the bi-linear constitutive relation is assumed.

From eqns (A1)–(A3), we have the second-order perturbation equations for each element

$$\ddot{f}_i^{\mathrm{I}} = k_{ij}^{\mathrm{II}} \ddot{u}_j^{\mathrm{I}} + k_{ij}^{\mathrm{I\,III}} \ddot{u}_j^{\mathrm{II}} + \hat{f}_i^{\mathrm{I}}, \tag{A4}$$

$$\hat{f}_i^{\mathrm{I}} = AL_0 \frac{\partial \varepsilon^{\mathrm{I}}}{\partial u_i^{\mathrm{I}}} \left(C^{\mathrm{II}} \frac{\partial^2 \varepsilon^{\mathrm{I}}}{\partial u_j^{\mathrm{I}} \partial u_k^{\mathrm{I}}} \dot{u}_j^{\mathrm{I}} \dot{u}_k^{\mathrm{I}} + C^{\mathrm{I\,II}} \frac{\partial^2 \varepsilon^{\mathrm{II}}}{\partial u_j^{\mathrm{II}} \partial u_k^{\mathrm{II}}} \dot{u}_j^{\mathrm{II}} \dot{u}_k^{\mathrm{II}} \right) + 2AL_0 \dot{\sigma}^{\mathrm{I}} \frac{\partial^2 \varepsilon^{\mathrm{I}}}{\partial u_i^{\mathrm{I}} \partial u_j^{\mathrm{I}}} \dot{u}_j^{\mathrm{I}} \tag{A5}$$

in which a hat indicates the variables expressed in terms of the first-order derivatives. Note that the coefficients k_{ij}^{II} and $k_{ij}^{\mathrm{I\,III}}$ are identical to those in eqn (31). We have the perturbation equations for the Γ^{II} state by replacing the superscripts I with II and II with I, respectively. Assembling the perturbation equations for the elements leads to the second-order perturbation equations for the total system

$$\ddot{\mathbf{F}}^{\mathrm{I}} = \mathbf{K}^{\mathrm{II}} \ddot{\mathbf{U}}^{\mathrm{I}} + \mathbf{K}^{\mathrm{I\,III}} \ddot{\mathbf{U}}^{\mathrm{II}} + \hat{\mathbf{F}}^{\mathrm{I}}, \tag{A6}$$

$$\ddot{\mathbf{F}}^{\mathrm{II}} = \mathbf{K}^{\mathrm{II\,I}}\ddot{\mathbf{U}}^{\mathrm{I}} + \mathbf{K}^{\mathrm{II\,II}}\ddot{\mathbf{U}}^{\mathrm{II}} + \hat{\mathbf{F}}^{\mathrm{II}}. \tag{A7}$$

Note again that the coefficient matrices are the same as those in the rate equations (37) and (38). These $2 \times 3N$ simultaneous linear equations (A6) and (A7) are to be solved using the boundary conditions after the value of $\ddot{\psi}$ is specified.

When the derivatives are employed up to the second order, the termination conditions (39)–(41) of the incremental step become quadratic equations of the step length $\Delta\tau$, while the conditions are linear equations when only the first derivatives are used. Besides these termination conditions, we must consider the conditions

$$\dot{\varepsilon}^{t}(\tau_{h+1}) = \dot{\varepsilon}^{t}(\tau_h) + \ddot{\varepsilon}^{t}(\tau_h)\Delta\tau = 0, \tag{A8}$$

$$\dot{\varepsilon}^{c}(\tau_{h+1}) = \dot{\varepsilon}^{c}(\tau_h) + \ddot{\varepsilon}^{c}(\tau_h)\Delta\tau = 0 \tag{A9}$$

for the transitions T → E and C → E, respectively.

Substituting the step length and the derivatives up to the second order into eqns (18)–(22), we obtain the values of the state variables at $\tau = \tau_{h+1}$.

Appendix B: Formulation and convergence criteria for response analysis

As a solution method for the response analysis, the incremental perturbation method (Yokoo et al., 1976) is used in this paper. In this method, the equilibrium path is traced using the higher-order derivatives up to the desired order with respect to the equilibrium path parameter t. Hence yielding and unloading can be predicted with the desired accuracy.

Differentiating the kinematic relations (1)–(3), we obtain the following equations

$$\varepsilon' = \frac{\partial \varepsilon}{\partial u_i} u_i' \tag{B1}$$

where prime indicates partial differentiation with respect to t. The equilibrium condition is written as

$$f_i' = AL_0 \left(\sigma' \frac{\partial \varepsilon}{\partial u_i} + \sigma \frac{\partial^2 \varepsilon}{\partial u_i \, \partial u_j} u_j' \right). \tag{B2}$$

The constitutive relation is expressed as

$$\sigma' = C\varepsilon' \tag{B3}$$

in which

$$C = E \quad \text{in the elastic range,} \tag{B4}$$

$$C = E_t, \quad \varepsilon' \geqslant 0 \quad \text{for the loading response in tension,} \tag{B5}$$

$$C = E, \quad \varepsilon' < 0 \quad \text{for the unloading response in tension,} \tag{B6}$$

$$C = E_t, \quad \varepsilon' \leqslant 0 \quad \text{for the loading response in compression,} \tag{B7}$$

$$C = E, \quad \varepsilon' > 0 \quad \text{for the unloading response in compression.} \tag{B8}$$

Differentiating eqn (5) with respect to t, we have the equations for each element

$$f'_i = k_{ij} u'_j, \tag{B9}$$

$$k_{ij} = C \frac{\partial \varepsilon}{\partial u_i} \frac{\partial \varepsilon}{\partial u_j} + \sigma \frac{\partial^2 \varepsilon}{\partial u_i \partial u_j}. \tag{B10}$$

By assembling the equations for each element, we obtain the equations for the total system as

$$\mathbf{F}' = \mathbf{K}\mathbf{U}'. \tag{B11}$$

Note that we should find the set of tangent stiffnesses that are consistent with the resulting signs of $\mathbf{E}'$. Differentiation of eqns (B1)–(B11) leads to higher-order perturbation equations. Solving the perturbation equations, we obtain the higher-order derivatives. An increment is terminated when yielding, unloading or load reversal occurs. In addition, the step length Δt is kept smaller than the maximum allowable value $\Delta \bar{t}_{\max}$ specified for preventing excessive accumulation of the truncation errors. Repeating these procedures, the equilibrium path is traced step by step.

In the numerical examples, the higher-order terms are employed up to the second order. The response is regarded to be divergent if buckling occurs or if one of the absolute maximum value of $\mathbf{U}$ exceeds the specified value $\bar{U}_{\max}$. On the other hand, the response is judged to be convergent when the following condition is satisfied.

$$\max \left| \frac{U_{n(l+1)} - U_{n(l)}}{U_{n(l)}} \right| < \bar{e} \quad (n = 1, 2, \ldots, 3N) \tag{B12}$$

where U_n is the nth component of $\mathbf{U}$, subscript l indicates the number of cycles and $\bar{e}$ is the specified value of the relative error. These values are set to be $\bar{U}_{\max} = 5$ cm, $\Delta \bar{t}_{\max} = 0.001$, and $\bar{e} = 1 \times 10^{-4}$ for the two-bar truss, and $\bar{U}_{\max} = 80$ cm, $\Delta \bar{t}_{\max} = 0.2$, and $\bar{e} = 1 \times 10^{-6}$ for the ten-bar truss.

Acknowledgement

This work was supported by JSPS Research Fellowships for Young Scientists.

References

Bathe, K.J., 1996. Finite Element Procedures. Prentice Hall, New Jersey.

Bazant, P.Z., Cedolin, L., 1991. Stability of Structures. Oxford University Press, New York.

Crisfield, M.A., 1991. Non-linear Finite Element Analysis of Solids and Structures, vol. 1. John Wiley and Sons, New York.

Crisfield, M.A., 1997. Non-linear Finite Element Analysis of Solids and Structures, vol. 2. John Wiley and Sons, New York.

Gross-Weege, J., 1990. A unified formulation of statical shakedown criteria for geometrically nonlinear problems. International Journal of Plasticity 6, 433–447.

Koiter, W.T., 1960. General theorems for elastic–plastic structures. In: Sneddon, J.N., Hill, R. (Eds.), Progress in Solid Mechanics, vol. 1. North Holland, Amsterdam, pp. 167–221.

König, J.A., 1987. Shakedown of Elastic–Plastic Structures. Elsevier, Amsterdam.
Maier, G., 1972. A shakedown matrix theory allowing for workhardening and second-order geometric effects. In: Sawczuk, A. (Ed.), Foundations of Plasticity, vol. 1. Noordhoff, Leyden, pp. 417–433.
Maier, G., Pan, L.G., Perego, U., 1993. Geometric effects on shakedown and ratchetting of axisymmetric cylindrical shells subjected to variable thermal loading. Engineering Structures 15, 453–465.
Nguyen, Q.S., Gary, G., Baylac, G., 1983. Interaction buckling–progressive deformation. Nuclear Engineering and Design 75, 235–243.
Hill, R., 1958. A general theory of uniqueness and stability in elastic–plastic solids. Journal of the Mechanics and Physics of Solids 6, 236–249.
Polizzotto, C., Borio, G., 1996. Shakedown and steady-state responses of elastic–plastic solids in large displacements. International Journal of Solids and Structures 33, 3415–3437.
Pycko, S., König, J.A., 1991. Steady plastic cycles on reference configuration in the presence of second-order geometric effects. European Journal of Mechanics, A/Solids 10, 301–321.
Shanley, F.R., 1947. Inelastic column theory. Journal of Aeronautical Sciences 14, 261–268.
Siemaszko, A., König, J.A., 1985. Analysis of stability of incremental collapse of skeletal structures. Journal of Structural Mechanics 13, 301–321.
Stumpf, H., 1993. Theoretical and computational aspects in the shakedown analysis of finite elastoplasticity. International Journal of Plasticity 9, 583–602.
Uetani, K., 1984. Symmetry limit theory and steady-state limit theory for elastic–plastic beam-columns subjected to repeated alternating bending. Thesis of Doctorat Engineering, Kyoto, in Japanese.
Uetani, K., 1989. Uniqueness criterion for incremental variation of steady state and symmetry limit. Journal of the Mechanics and Physics of Solids 37, 495–514.
Uetani, K., 1991. Cyclic plastic collapse of steel planar frames. In: Fukumoto, Y., Lee, G. (Eds.), Stability and Ductility of Steel Structures under Cyclic Loading. CRC Press, pp. 261–271.
Uetani, K., Nakamura, T., 1983. Symmetry limit theory for cantilever beam-columns subjected to cyclic reversed bending. Journal of the Mechanics and Physics of Solids 31, 449–484.
Weichert, D., 1986. On the influence of geometrical nonlinearities on the shakedown of elastic–plastic structures. International Journal of Plasticity 2, 135–148.
Yokoo, Y., Nakamura, T., Uetani, K., 1976. The incremental perturbation method for large displacement analysis of elastic–plastic structures. International Journal for Numerical Methods in Engineering 10, 503–525.